Generation of a time-frequency grid state with integrated biphoton frequency combs

N. Fabre,[1,*] G. Maltese,[1] F. Appas,[1] S. Felicetti,[1] A. Ketterer,[1,2] A. Keller,[3] T. Coudreau,[1] F. Baboux,[1] M. I. Amanti,[1] S. Ducci,[1] and P. Milman[1]

[1]*Laboratoire Matériaux et Phénomènes Quantiques, Sorbonne Paris Cité, Université de Paris, CNRS UMR 7162, 75013 Paris, France*

[2]*Physikalisches Institut, Albert-Ludwigs-Universität Freiburg, Hermann-Herder-Strasse 3, 79104 Freiburg, Germany*

[3]*Laboratoire Matériaux et Phénomènes Quantiques, Sorbonne Paris Cité, Université de Paris, Université Paris Saclay, CNRS UMR 7162, 75013 Paris, France*

(Received 12 April 2019; accepted 3 June 2020; published 6 July 2020)

Encoding quantum information in continuous variables is intrinsically faulty. Nevertheless, redundant qubits can be used for error correction, as proposed by Gottesman *et al.* [Phys. Rev. A **64** 012310 (2001)]. We show how to experimentally implement this encoding using time-frequency continuous degrees of freedom of photon pairs produced by spontaneous parametric down conversion. We illustrate our results using an integrated AlGaAs photon-pair source. We show how single-qubit gates can be implemented and finally propose a theoretical scheme for correcting errors in circuit-like and measurement-based architectures.

DOI: 10.1103/PhysRevA.102.012607

I. INTRODUCTION

Quantum information can be encoded in qubits corresponding to discrete quantum states of physical systems, such as atomic electronic states or the polarization of single photons. The essence of quantum computation (QC) is to manipulate qubits with a universal set of unitary quantum gates [1,2]. A fundamental ingredient for QC, inherited from classical computation, is error correction. In the realm of quantum computing, quantum error correction (QEC) [3,4] fights against a fundamental aspect of quantum systems: their fragility to keep quantum properties at large scale and for a long time that, usually, depends on the size of the system. Ingenious solutions to this problem consist in encoding a qubit of information in particular states composed of more than one physical qubit. The resulting logical qubits enabling QEC depend on the type of errors that are more likely to affect the system. For instance, a code that corrects for qubit flips, dephasing, and all the errors created by the combination of these involves the creation of a complex five-qubit entangled state whose symmetries enable the detection and correction of the mentioned errors [5].

If one considers harmonic oscillators or analogous systems, as, for instance, two quadratures of the electromagnetic field, encoding quantum information in continuous variable (CV) is in principle possible using any two orthogonal states of a given quadrature [6]. However, such states are nonphysical, and the closest one can get to them is by considering squeezed states [7], which are sub-shot-noise states. As a matter of fact, squeezed states can be considered as noisy quadrature eigenstates, where the noise is modeled by products of displacement operators in phase space weighted by Gaussian functions representing the probability amplitude distribution of these displacements. Physical states described by continuous variables are thus intrinsically noisy and, within this picture, displacements in phase space are the main source of noise for such encoding. Moreover, since all physical states are noisy, errors propagate throughout quantum operations and must be corrected regularly. This picture is particularly suitable to a number of relevant physical systems, as the quantum state produced by optical parametric oscillators (OPO) [8–10] and continuous degrees of freedom of photon pairs, as discussed in the present paper. The problem of correction from displacement errors was considered by Gottesman, Kitaev and Preskill (GKP), who introduced what we refer now on as GKP states [11], which are qubits defined in CV displaying a periodic structure.

In spite of the importance of GKP states in quantum information with CV [12–14], their experimental engineering remains extremely difficult in quantum optics [15–17]. They correspond to highly non-Gaussian states composed of the coherent superposition of several delocalized states. The engineering of non-Gaussian states using OPOs is still challenging, and even if some experiments have demonstrated it [18–20] they involve single photon addition and/or subtraction through postselection. As a consequence, one of the major advantages of using such systems, determinacy, is lost. Also, the generated non-Gaussian states are still far from the physical GKP states. Recently, such states have been produced using the motional states of one trapped ion [21], in superconducting qubits [22], and for other platforms [23–25].

In the present paper, we show that biphoton frequency combs produced by intracavity spontaneous parametric down conversion (SPDC) can be used to experimentally generate, manipulate, and detect grid states encoded in time (t) and frequency (ω). We propose a method to implement a fundamental operation of quantum error correction. Our results rely on the analogy between quantum states composed of many photons in one mode of the electromagnetic field and one photon that can occupy a continuum of frequency modes, which is the continuous degree of freedom we consider here.

*nicolas.fabre@univ-paris-diderot.fr

We show that the time-frequency phase space at the single-photon level has the same noncommutative structure as the usual quadrature position-momentum phase space. Our results are experimentally illustrated using an AlGaAs nonlinear cavity producing photon pairs by SPDC at room temperature and telecom wavelengths that are compliant with electrical injection [26]. The proposed scheme is not specific to the considered platform and it could be implemented with other quantum-optical setups, such as those in Refs. [27,28].

This paper is organized as follows. We start in Sec. II by describing the properties of the time-frequency phase space of a single photon and describe its quantum structure and properties. We use these results to properly introduce the chronocyclic Wigner distribution. In Sec. III, we define the time-frequency GKP states, or more generally the time-frequency grid states [23], which are fully analogous to the ones made from position-momentum quadrature states [11]. Following the formalism developed, we mathematically introduce the two-dimensional (2D) time-frequency GKP state. In Sec. IV A, we present an experimental implementation of our results in a chip-integrated source consisting of a AlGaAs Bragg reflector waveguide generating a 2D time-frequency grid state, and in Sec. IV B we show how such states can be used for correcting time-frequency shift errors. This state can be experimentally manipulated and characterized using Hong-Ou and Mandel (HOM) interferometry [29], as shown in Sec. IV C. Finally, in Sec. IV D, we theoretically propose a simple experimental scheme based on photon detection to implement quantum error correction for time-frequency GKP states.

II. TIME-FREQUENCY PHASE SPACE OF A SINGLE PHOTON

In this section, we introduce the time-frequency phase space of a single photon, following the construction of the usual nonrelativistic phase space in quadrature position-momentum variable. For the sake of completeness and to clarify the analogy with the traditional quadrature position-momentum CV, we also mention some results of this formalism.

A. Time-frequency phase space description

In order to fix the notation, the photon creation operator at frequency ω acts on the vacuum $|0\rangle$ as

$$\hat{a}^\dagger(\omega)|0\rangle = |1_\omega\rangle = |\omega\rangle. \tag{1}$$

We thus have that $|1_\omega\rangle$ and $|\omega\rangle$ are equivalent notations for a single photon at frequency ω. In the present paper, we will be mostly interested in the single-photon subspace and so we will use the simplified notation $|\omega\rangle$. We can also define an annihilation operator fore the mode ω as $\hat{a}(\omega)|\omega\rangle = |0\rangle$. If we consider only the frequency degree of freedom, the creation and annihilation operators obey the bosonic commutation relation:

$$[\hat{a}(\omega), \hat{a}^\dagger(\omega')] = \delta(\omega - \omega')\mathbb{I}, \tag{2}$$

where $\mathbb{I}$ is the identity operator. Analogously, we define the creation operator for a single photon at time t, $\hat{a}^\dagger(t)$, where t is the time interval elapsed from the photon's creation at the source and its arrival at the detector. The creation operator $\hat{a}^\dagger(t)$ can be obtained from a Fourier transform of $\hat{a}^\dagger(\omega)$:

$$\hat{a}^\dagger(t) = \frac{1}{\sqrt{2\pi}} \int_{\mathbb{R}} d\omega e^{i\omega t} \hat{a}^\dagger(\omega), \tag{3}$$

and we have that $|t\rangle = |1_t\rangle = \hat{a}^\dagger(t)|0\rangle = \frac{1}{\sqrt{2\pi}} \int_{\mathbb{R}} d\omega e^{i\omega t}|\omega\rangle$.

Since $\{|\omega\rangle\}$ is an orthogonal basis, we can expand a pure single-photon state $|\Psi\rangle$ in this basis:

$$|\Psi\rangle = \int_{\mathbb{R}} S(\omega) d\omega |\omega\rangle, \tag{4}$$

where $S(\omega)$ is the amplitude spectrum of the single photon, with the normalization condition $\int_{\mathbb{R}} |S(\omega)|^2 d\omega = 1$.

We also consider single photons with a temporal structure, described by the state

$$|\Psi\rangle = \int_{\mathbb{R}} \tilde{S}(t) dt |t\rangle, \tag{5}$$

where $\tilde{S}(t)$ is the Fourier transform of the amplitude spectrum $S(\omega)$ of the source. Free space propagation for a time t leads to the evolution of the creation operator: $\hat{a}_t^\dagger(\omega) = e^{-i\omega t}\hat{a}^\dagger(\omega)$, and the wave function at time t reads

$$|\Psi(t)\rangle = \int_{\mathbb{R}} S(\omega) e^{-i\omega t} d\omega |\omega\rangle. \tag{6}$$

Rigorously, the integration range in Eqs. (6) and (4) should be $\mathbb{R}^+$. We have extended it to $\mathbb{R}$ as we consider experiments where the amplitude spectrum fulfills $S(\omega \leqslant 0) = 0$. In the experimental setup we implement in this paper, $S(\omega)$ is typically nonzero only in the telecom wavelength.

The above definitions [Eqs. (1)–(6)] are completely analogous to the ones commonly defined in the case of a monomode multiphoton electromagnetic field, modeled by a quantum harmonic oscillator. Indeed, the quantized electromagnetic field is described by quadratures $\hat{X}$ and $\hat{P}$ defined by

$$\hat{X} = \sqrt{\frac{\hbar}{2\omega}}(\hat{a} + \hat{a}^\dagger), \tag{7}$$

$$\hat{P} = -i\sqrt{\frac{\hbar\omega}{2}}(\hat{a} - \hat{a}^\dagger), \tag{8}$$

where ω is the frequency of the field and $\hat{a}, \hat{a}^\dagger$ are the annihilation-creation operators (implicitly at the frequency ω) which obey the commutation relation $[\hat{a}, \hat{a}^\dagger] = \mathbb{I}$. $\hat{X}$ and $\hat{P}$ admit real eigenvalues noted as x and p, called the position and momentum quadratures. The associated eigenvectors $|x\rangle, |p\rangle$ are analogous to the state $|\omega\rangle$ defined by Eq. (1) and the state $|t\rangle$. Since they are canonical conjugate variable, $|x\rangle, |p\rangle$ are related by a Fourier transform:

$$|x\rangle = \frac{1}{\sqrt{2\pi\hbar}} \int_{\mathbb{R}} e^{-ixp/\hbar}|p\rangle dp, \tag{9}$$

which is equivalent to Eq. (3) after applying it to the vacuum state $|0\rangle$ on both sides the equation. The position and momentum basis are orthogonal and complete as the frequency and time basis of a single photon. Also, they are not physical since they correspond to infinitely squeezed (in position or momentum state) and not square normalizable [1]. They

are nonetheless useful for building physical states with a finite squeezing in both position and momentum variables, described by the wave function

$$|\psi\rangle = \int dx \psi(x)|x\rangle. \tag{10}$$

In conclusion, the state described by Eq. (10) is perfectly mathematically analogous to Eq. (4). $|\psi(x)|^2$ represents the quadrature position probability distribution and is normalized to unity, as $|S(\omega)|^2$ describes the spectrum probability distribution. In the following, we will set the Planck's constant $\hbar$ to one.

1. Time-frequency Wigner distribution for a single photon

We now define the time-frequency Wigner distribution. The Wigner distribution in phase space can be seen as the expectation value of the parity operator [30] or, equivalently, as the inverse Fourier transform of a characteristic function. The latter is constructed using a symmetric ordering of bosonic operators. We will proceed analogously, by introducing the displacement frequency mode operator in the single-photon subspace.

Using the previously introduced bosonic operators, we can define the displacement mode operator in frequency as

$$\hat{D}(\mu) = \int \hat{a}^\dagger(\omega+\mu)\hat{a}(\omega)d\omega. \tag{11}$$

Analogously, for the displacement in time we can write

$$\hat{\mathcal{D}}(\tau) = \int \hat{a}^\dagger(t+\tau)\hat{a}(t)dt. \tag{12}$$

As for Eq. (6), we have extended the range of integration from $\mathbb{R}^+$ to $\mathbb{R}$. Indeed, for the envisaged application, μ will be small enough so that the resulting displaced state amplitude spectrum $S(\omega)$ will have its support in $\mathbb{R}^+$.

Displacement operators do not commute, and we obtain the Weyl relation,

$$\hat{D}(\mu)\hat{\mathcal{D}}(\tau) = e^{i\mu\tau}\hat{\mathcal{D}}(\tau)\hat{D}(\mu). \tag{13}$$

Using the commutation relations, in analogy with the quadrature position-momentum phase space case, we can identify different possible orderings of the operators: the normal order $\hat{D}_n(\mu,\tau) = \hat{D}(\mu)\hat{\mathcal{D}}(\tau)$, the antinormal order $\hat{D}_{an}(\mu,\tau) = \hat{\mathcal{D}}(\tau)\hat{D}(\mu)$, and the symmetric order, $\hat{D}_s(\mu,\tau) = \hat{D}(\mu)\hat{\mathcal{D}}(\tau)e^{-i\tau\mu/2}$.

For a monomode multiphoton field, the quadrature position-momentum displacement operator in the symmetric ordering is defined by

$$\hat{D}_s(x,p) = e^{-ixp/2}e^{-i\hat{X}p}e^{i\hat{P}x}. \tag{14}$$

The position displacement operator $e^{i\hat{P}x'}$ acts on the position and momentum kets as $e^{i\hat{P}x'}|x\rangle = |x+x'\rangle$ and $e^{i\hat{P}x'}|p\rangle = e^{ipx'}|p\rangle$ and have a similar algebra to that of the frequency displacement operator which acts on the frequency and time state $\hat{D}(\mu)|\omega\rangle = |\omega+\mu\rangle$ and $\hat{D}(\mu)|t\rangle = e^{i\mu t}|t\rangle$.

Even though the quadrature position-momentum displacement operators $\hat{D}_s(x,p)$ have the same algebraic properties than the time-frequency ones, they do not have the same mathematical representation. An exponential representation of the time-frequency displacement operators [see Eq. (14)] would require the introduction of a time operator. We point out that such operator was introduced recently in Ref. [31], but a quantum reference frame (a quantum clock) is needed and allows us to avoid considering time as a conditioned quantity. Nevertheless, the formalism introduced [31] is not necessary in the mathematical treatment dealt in this paper.

We return to the study of the time-frequency phase space of a single photon. All the following properties and definitions are borrowed from the quadrature position-momentum formalism, since we showed the mathematical analogies between these two sets of continuous variables, within the displacement operators. The unitary displacement operators $\hat{D}_\xi$, irrespective of the ordering, $\xi = s, an, n$, obey the following orthogonality relation:

$$\mathrm{Tr}[\hat{D}_\xi^\dagger(\mu,\tau)\hat{D}_\xi(\mu',\tau')] = \delta(\tau'-\tau)\delta(\mu'-\mu), \tag{15}$$

and the completeness relation

$$\iint d\mu d\tau \hat{D}_\xi(\mu,\tau)\hat{D}_\xi^\dagger(\mu,\tau) = \mathbb{I}. \tag{16}$$

Using Eqs. (15) and (16), we can expand all Hermitian matrices in this orthogonal basis, and thus the density matrix reads

$$\hat{\rho} = \iint \chi_{\rho,\xi}(\mu,\tau)\hat{D}_\xi(\mu,\tau)d\mu d\tau. \tag{17}$$

The coordinate function $\chi_{\rho,\xi}(\mu,\tau) = \mathrm{Tr}(\hat{\rho}\hat{D}_\xi^\dagger(\mu,\tau))$ is called the characteristic function, and it can be normal, antinormal, or symmetric depending on the ordering of the displacement operator. The Fourier transform of the characteristic function leads to a quasiprobability distribution. In particular, using the symmetric characteristic distribution, one can obtain the chronocyclic Wigner distribution,

$$W(\omega,t) = \frac{1}{\sqrt{2\pi}}\int d\omega' e^{2i\omega' t}\langle\omega-\omega'|\hat{\rho}|\omega+\omega'\rangle. \tag{18}$$

The chronocyclic Wigner distribution gives the same information as the associated density matrix, following the completeness property. This distribution is also normalized: $\iint dtd\omega W(\omega,t) = \mathrm{Tr}(\hat{\rho}) = 1$. In the case of a pure state $\hat{\rho} = |\psi\rangle\langle\psi|$ characterized by its amplitude spectrum $S(\omega)$ [see Eq. (4)], the chronocylic Wigner distribution can be written as

$$W(\omega,t) = \frac{1}{\sqrt{2\pi}}\int d\omega' e^{2i\omega' t}S(\omega-\omega')S^*(\omega+\omega'). \tag{19}$$

The marginals of the Wigner distribution lead to different physically measurable quantities such as the spectrum of the source,

$$\int W(\omega,t)dt = |S(\omega)|^2, \tag{20}$$

and the distribution of the arrival time of the photon of the source (using a fixed origin of time),

$$\int W(\omega,t)d\omega = |\tilde{S}(t)|^2. \tag{21}$$

We can also see the chronocyclic Wigner distribution here as the expectation value of the displaced parity operator by

applying the same methods as in Ref. [30] using the symmetric displacement operator $\hat{D}_s$,

$$W(\omega, t) = \mathrm{Tr}(\hat{\rho}\hat{D}_s(\omega, t)\hat{\Pi}\hat{D}_s^{\dagger}(\omega, t)), \tag{22}$$

where $\hat{\Pi}$ is the parity operator which acts on a frequency state as $\hat{\Pi}|\omega\rangle = |-\omega\rangle$. Consequently, measuring the chronocyclic Wigner distribution at the origin is a measurement of the average value of the parity operator.

Finally, it can be shown that the chronocyclic Wigner distribution obeys the Stratonovich-Weyl rules [32,33].

Owing to the noncommutativity of the bosonic operator Eq. (2) and, consequently, the noncommutativity of the displacement operators [see Eq. (13)], the time-frequency phase space of a single photon is noncommutative, as the quadrature position-momentum phase space. It leads to the analogy between one single photon in many frequency modes and many photons in one frequency mode.

The introduced Wigner distribution can be generalized to the situation where more than one photon occupy different frequency modes. We will describe in details the two-photon case in the next section.

2. Wigner distribution of two photons and associated marginals

For a two-photon state, the wave function can be written as

$$|\psi\rangle = \iint d\omega_s d\omega_i F(\omega_s, \omega_i)|\omega_s, \omega_i\rangle, \tag{23}$$

where F denotes the joint spectral amplitude and $\omega_s(\omega_i)$ is the frequency of the signal (idler) photon. The Wigner distribution of a pure state $|\psi\rangle$ is

$$\begin{aligned} &W(\omega_s, \omega_i, t_s, t_i) \\ &= \iint d\omega' d\omega'' e^{2i\omega' t_s} e^{2i\omega'' t_i} \langle \omega_s - \omega', \omega_i - \omega'' || \psi \rangle \\ &\quad \times \langle \psi || \omega_s + \omega', \omega_i + \omega'' \rangle, \end{aligned} \tag{24}$$

with marginals

$$\iint W(\omega_s, \omega_i, t_s, t_i) dt_s dt_i = |F(\omega_s, \omega_i)|^2. \tag{25}$$

We also have

$$\iint W(\omega_s, \omega_i, t_s, t_i) d\omega_s d\omega_i = |H(t_s, t_i)|^2, \tag{26}$$

which corresponds to the joint temporal intensity, which is the probability of measuring a photon at an arrival time t_s in one detector and a photon at an arrival time t_i in another detector, H is the corresponding probability amplitude. We can also define two other "crossed" marginals: the probability to detect one photon at the arrival time t_s (resp. t_i) and the other at the frequency ω_i (resp. ω_s). The measurement of the four marginals and the reconstruction of the joint spectral amplitude has been performed in Ref. [34]; however, this technique cannot be applied to all optical systems and depend on the spectral width of the considered joint spectral amplitude.

In the next section, we use the formalism presented here to analyze the phase space distribution and representation for some relevant quantum states. As a first example, we will describe coherent-like state in time-frequency variables. Then, we will address grid and GKP state formed with one and two photons.

III. TIME-FREQUENCY GRID STATES

Before introducing grid states, we describe coherent-like states in time-frequency phase space.

A. Coherent-like state in time-frequency variables

The coherent state is a specific state of the monomode multiphoton field. Its wave function in the position basis [35] can be written as

$$|x_0, p_0\rangle = \int_{\mathbb{R}} dx e^{-(x-x_0)^2} e^{ixp_0} |x\rangle. \tag{27}$$

The associated Wigner distribution in the (x, p) phase space is a Gaussian centered at (x_0, p_0). The analogy between the mathematical structure of frequency states of single photons and the quadratures' position-momentum state motivates the definition of the coherent-like state $|\frac{\omega_1}{\Delta\omega}, \tau\Delta\omega\rangle$ as a single-photon state with a Gaussian amplitude spectrum:

$$\left|\frac{\omega_1}{\Delta\omega}, \tau\Delta\omega\right\rangle = \int d\omega e^{-(\omega-\omega_1)^2/(2\Delta\omega^2)} e^{i\omega\tau} |\omega\rangle, \tag{28}$$

where ω_1 and τ are two parameters representing the average value of the chronocyclic Wigner distribution and $\Delta\omega$ is the spectral width of the Gaussian spectrum. As in the usual phase-space representation, the coherent-like state also forms an overcomplete basis.

The physical interpretations of the coherent and coherent-like frequency time state are very different. The coherent state $|x_0, p_0\rangle$, also noted $|\alpha\rangle$ with $\mathrm{Re}(\alpha) = x_0$ and $\mathrm{Im}(\alpha) = p_0$, is the eigenvector of the annihilation operator $\hat{a}$ with the corresponding complex eigenvalue α. $|\alpha|^2$ is the average value of the photon number $\langle \hat{a}^{\dagger}\hat{a} \rangle$ of the monomode multiphoton field. Also, the free evolution trajectory in the quadrature position-momentum phase space of a coherent state is a circle, as the classical harmonic oscillator, which justify its name. For the coherent-like time-frequency state, the average value of the photon number is one, since it is a single photon and the trajectory of a free evolution in time-frequency phase space is a translation along the time axis. The aim of these remarks highlight the main physical difference between these two states, despite their mathematical analogies.

B. Grid states

We now use the formalism developed in the previous section to introduce the time-frequency grid state and, more specifically, the time-frequency GKP state. We also show their application for time-frequency quantum error correction.

Grid states were first defined using quadrature position-momentum continuous variables [11,36] and correspond to a two-dimensional lattice in phase space where the area of the unit cell is a multiple of 2π. Time-frequency grid states also verify the following property: They are periodic structures formed by the superposition of many modes of a single photon. Such states are mathematically equivalent to the quadrature position-momentum ones due to the

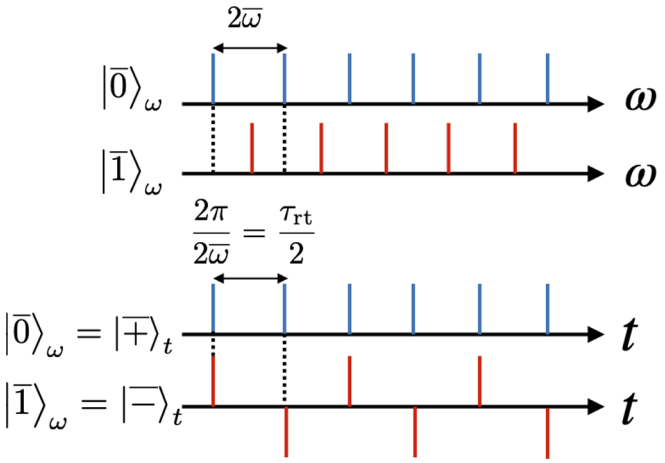

FIG. 1. Time-frequency GKP state in the frequency and time bases.

noncommutative algebra of the time-frequency displacement operators.

More precisely, the time-frequency grid state is defined as a common eigenstate with the eigenvalue $+1$ of the two commuting operators $\hat{D}(\omega)$ and $\hat{\mathcal{D}}(t)$ when the product of the two parameters verify $\omega t = 0 \bmod 2\pi$. This property allows us to measure both the time and the frequency modulo 2π. The wave function of a general grid state can be written as

$$|\psi\rangle = \sum_{n\in\mathbb{Z}} |\sqrt{\pi}(2n+\mu)\rangle_\omega, \tag{29}$$

where μ is an integer. The $+1$ eigenspace of the displacement operators is two dimensional and allows us to define a qubit taking for instance the values $\mu = 0$ and 1. It is developed in more details in the following paragraph.

C. Time-frequency GKP state

1. Definition and notation

We start by providing the general framework to define single-photon GKP states with many frequency modes. The two possible states of the qubit are the eigenstates of the displacement operators $\hat{D}(2\overline{\omega})$, $\hat{\mathcal{D}}(\frac{2\pi}{2\overline{\omega}})$, also called the stabilizer of the code (see Fig. 1):

$$|\overline{0}\rangle_\omega = \sum_{n\in\mathbb{Z}} \left|\frac{\omega_p}{2} + 2n\overline{\omega}\right\rangle, \tag{30}$$

$$|\overline{1}\rangle_\omega = \sum_{n\in\mathbb{Z}} \left|\frac{\omega_p}{2} + (2n+1)\overline{\omega}\right\rangle. \tag{31}$$

In the above, $2\overline{\omega}$ is the periodicity of the state and $\omega_p/2$ is a constant that will be later associated to a physical parameter. These states are called time-frequency square GKP states, because their time-frequency phase space representation is squared [37]. For simplicity, we will call them simply time-frequency GKP states.

Alternatively, as we show in Fig. 1, we can use the time representation of the GKP states (up to normalization):

$$|\overline{0}\rangle_\omega = \tau_{\rm rt} \sum_{n\in\mathbb{Z}} e^{i\frac{\omega_p}{2}\frac{n\tau_{\rm rt}}{2}} \left|\frac{n\tau_{\rm rt}}{2}\right\rangle = |\overline{+}\rangle_t, \tag{32}$$

$$|\overline{1}\rangle_\omega = \tau_{\rm rt} \sum_{n\in\mathbb{Z}} e^{i\frac{\omega_p}{2}\frac{n\tau_{\rm rt}}{2}} (-1)^n \left|\frac{n\tau_{\rm rt}}{2}\right\rangle = |\overline{-}\rangle_t, \tag{33}$$

where $\tau_{\rm rt} = \frac{2\pi}{\overline{\omega}}$. Here we have used that $\sum_{n\in\mathbb{Z}} e^{2in\pi t/\tau_{\rm rt}} = \tau_{\rm rt}\sum_{n\in\mathbb{Z}} \delta(t - n\tau_{\rm rt})$. If we have the equality $\exp(i\frac{\omega_p}{2}\frac{n\tau_{\rm rt}}{2}) = 1$, which corresponds to the condition that ω_p is a multiple of $\overline{\omega}$, we can define a qubit. It will be the case in the experimental configuration specified in the next section. For the sake of simplicity, we will now set $\omega_p = 0$. The $|\overline{0}\rangle_t$, $|\overline{1}\rangle_t$ logical time GKP state [the eigenstates of the stabilizer $\hat{\mathcal{D}}(\tau_{\rm rt})$] are then (up to normalization)

$$|\overline{0}\rangle_t = \tau_{\rm rt} \sum_{n\in\mathbb{Z}} \left|\frac{2n\tau_{\rm rt}}{2}\right\rangle = |\overline{+}\rangle_\omega, \tag{34}$$

$$|\overline{1}\rangle_t = \tau_{\rm rt} \sum_{n\in\mathbb{Z}} \left|\frac{(2n+1)\tau_{\rm rt}}{2}\right\rangle = |\overline{-}\rangle_\omega, \tag{35}$$

where we have introduced $|\overline{\pm}\rangle_t = \frac{1}{\sqrt{2}}(|\overline{0}\rangle_t \pm |\overline{1}\rangle_t)$ and analogously for $|\overline{+}\rangle_\omega$.

The time-frequency phase space representation of the time-frequency GKP state is analogous to the GKP state in the (x, p) phase plane [11]. The wave function of the coherent superposition $|\overline{+}\rangle_\omega$, with the amplitude spectrum $S(\omega) = \sum_{n\in\mathbb{Z}}\langle\omega||n\overline{\omega}\rangle = \sum_{n\in\mathbb{Z}}\delta(\omega - n\overline{\omega})$ has the following chronocyclic Wigner distribution:

$$\begin{aligned} W(\omega,t) &= \int_{\mathbb{R}} d\omega' e^{2i\omega' t} S(\omega-\omega')S^*(\omega+\omega') \\ &= \sum_{n,m\in\mathbb{Z}^2} (-1)^{nm}\delta\left(t - \frac{\pi}{\overline{\omega}}n\right)\delta\left(\omega - \frac{\omega_p}{2} - \frac{\overline{\omega}}{2}m\right). \end{aligned} \tag{36}$$

This shows that the chronocyclic Wigner distribution is negative when n, m are both odd. Also, such states are not physical since we are summing over an infinite number of perfectly well-defined frequency (or time) modes.

2. Physical time-frequency GKP state

In this section, we will see how to formally describe physical (intrinsically noisy) time-frequency GKP states and how to physically interpret their number of peaks and the uncertainty of each mode. For that, we apply the formalism introduced in Ref. [38].

Physical time-frequency GKP states are constructed by applying a Kraus-like operator $\hat{\xi}$ to the ideal time-frequency GKP state:

$$|\tilde{0}\rangle_\omega = \hat{\xi}|\overline{0}\rangle_\omega = \iint d\omega dt \xi(\omega,t)\hat{\mathcal{D}}(t)\hat{D}(\omega)|\overline{0}\rangle_\omega. \tag{37}$$

If we suppose that frequency and time noise are uncorrelated Gaussian distribution, we have that $\xi(\omega,t) = G_{\delta\omega}(\omega)G_\kappa(t) = e^{-\omega^2/2\delta\omega^2}e^{-t^2/2\kappa^2}$. The physical interpretation of these two Gaussian noises becomes clearer after performing the time

integral in Eq. (37), which leads to

$$|\tilde{0}\rangle_\omega = \sum_{n\in\mathbb{Z}} \int T_{2n}(\omega) e^{-\omega^2\kappa^2/2} |\omega\rangle d\omega, \tag{38}$$

with $T_n(\omega) = \exp(-(\omega - n\overline{\omega})^2/(2\delta\omega^2))$ and we have used $\hat{\mathcal{D}}(t)\hat{D}(\omega)|\bar{0}\rangle_\omega = \sum_n e^{it(n\overline{\omega}+\omega)}$. In our terminology, time noise creates an envelope, limiting the number of relevant frequency modes while frequency noise introduces an intrinsic width to each peak. Alternatively, we can construct the physical GKP state by permuting the time and frequency displacement operators. Since they are noncommuting operators, the state obtained by this procedure is not the same as Eq. (38). For a quadrature position-momentum GKP state, the Kraus operator applied on ideal GKP state [24,38] models the finite width (which corresponds to the finite amount of squeezing or its inherent noise) of each position peak and of the total envelope. These Kraus operators are simply the unitary squeezing operators. Here, our Kraus-like operator modeled the bandwidth of the frequency peaks and the total envelope of the single-photon state but could also be used to describe the bandwidth of a coherent state. In both cases, quadrature position-momentum variable for a multiphoton field or time-frequency degree of freedom of single photon, the Kraus operators are unitary and do not alter the purity of the state.

The physical origin of the finite width of the time and frequency distribution are considered in our formalism as errors that can be due to the propagation of single photons in a dispersive medium, as an optical fiber. They can also be related to time and frequency uncertainties inherent to the state preparation process, as is the case of the setup presented in Sec. IV.

D. The 2D entangled time-frequency GKP state: Some useful mathematical tools

We now move to the two-qubit case and show how two GKP states can be entangled in time and frequency degrees of freedom. We start by considering an ideal separable two-photon state, a two-dimensional GKP state, that can be written as

$$\begin{aligned}|\overline{+}\rangle_{\omega_s}|\overline{+}\rangle_{\omega_i} = \tfrac{1}{2}(&|\bar{0}\rangle_{\omega_s}|\bar{0}\rangle_{\omega_i} + |\bar{0}\rangle_{\omega_s}|\bar{1}\rangle_{\omega_i} \\ &+ |\bar{1}\rangle_{\omega_s}|\bar{0}\rangle_{\omega_i} + |\bar{1}\rangle_{\omega_s}|\bar{1}\rangle_{\omega_i}).\end{aligned} \tag{39}$$

As in the one-qubit case, physical qubits can be constructed from (39) using the noise model introduced previously, based on the application of Kraus-like operators:

$$\begin{aligned}&|\tilde{\overline{+}}\rangle_{\omega_s}|\tilde{\overline{+}}\rangle_{\omega_i} \\ &= \iint dtdt' \hat{\mathcal{D}}_{\rm s}(t)\hat{\mathcal{D}}_{\rm i}(t') G_{1/\Delta\omega_p}(t) G_{1/\Delta\omega_-}(t') \\ &\quad\times \iint \hat{D}_{\rm s}(\omega)\hat{D}_{\rm i}(\omega') G_{\delta\omega_s}(\omega) G_{\delta\omega_i}(\omega') d\omega d\omega' |\overline{+}\rangle_{\omega_s}|\overline{+}\rangle_{\omega_i}.\end{aligned} \tag{40}$$

The functions $G_\alpha(x)$ are Gaussians of width α corresponding to the noise distribution on variables x. Using a calculation similar to that in Sec. III C 2, the corresponding joint spectral intensity of the state Eq. (40) has an elliptical envelope elongated along the ω_s or ω_i axis if $\Delta\omega_p < \Delta\omega_-$ or $\Delta\omega_- < \Delta\omega_p$ and is composed of circular cavity peaks of radius $\delta\omega$.

Frequency (or time) entanglement can be created by the application of a symmetric controlled-NOT (CNOT) operator $\hat{C}'$ that performs the following operation:

$$\hat{C}'|t_s, t_i\rangle = |t_s + t_i\rangle|t_s - t_i\rangle. \tag{41}$$

Equivalently, $\hat{C}'|\omega, \omega'\rangle = |\frac{\omega+\omega'}{2}, \frac{\omega-\omega'}{2}\rangle$. This gate operates in an analogous way to a balanced beam splitter that acts on the frequency or time degree of freedom instead of the field's quadratures [39]. We mention that the CNOT gate $\hat{C}$ acts on the position quadrature $|x, y\rangle$ as $\hat{C}|x, y\rangle = |x + y, x - y\rangle$ and corresponds to the transformation of a balanced beam splitter.

The entangling gate $\hat{C}'$ transforms displacement operators as follows:

$$\hat{C}'\hat{\mathcal{D}}_{\rm s}(t)\hat{\mathcal{D}}_{\rm i}(t')\hat{C}'^{-1} = \hat{\mathcal{D}}_{\rm s}\left(\frac{t+t'}{2}\right)\hat{\mathcal{D}}_{\rm i}\left(\frac{t-t'}{2}\right). \tag{42}$$

Such entangling gate is physically produced by a nonlinear effect that occurs naturally in the optical device we study here, as we will see in the next section.

We now consider a particular time-frequency noise model. It is obtained by first applying the frequency noise described by the Kraus-like operator on the ideal time-frequency 2D GKP state $|\psi\rangle_1 = (\iint \hat{D}_{\rm s}(\omega)\hat{D}_{\rm i}(\omega') G_{\delta\omega}(\omega) G_{\delta\omega}(\omega') d\omega d\omega')|\overline{+}\rangle_{\omega_s}|\overline{+}\rangle_{\omega_i}$. The associated joint spectral intensity of the state $|\psi\rangle_1$ is an infinite square grid, where each frequency peak is circular with radius $\delta\omega$. The state is still unphysical, since the frequency envelope along both frequency directions is infinite. Then, the envelop of the joint spectral intensity of the two-photon state is described by application of the correlated time noise, using the Kraus-like operator: $\iint \hat{\mathcal{D}}_{\rm s}(\frac{t+t'}{2})\hat{\mathcal{D}}_{\rm i}(\frac{t-t'}{2}) G_{1/\Delta\omega_p}(t) G_{1/\Delta\omega_-}(t') dt dt'$ on state $|\psi_1\rangle$. After these two operations, the wave function $|\psi\rangle_2$ describing the two-photon state can be written as

$$\begin{aligned}&|\psi\rangle_2 \\ &= \iint \hat{\mathcal{D}}_{\rm s}\left(\frac{t+t'}{2}\right)\hat{\mathcal{D}}_{\rm i}\left(\frac{t-t'}{2}\right) G_{1/\Delta\omega_p}(t) G_{1/\Delta\omega_-}(t') dt dt' \\ &\quad\times \iint \hat{D}_{\rm s}(\omega)\hat{D}_{\rm i}(\omega') G_{\delta\omega}(\omega) G_{\delta\omega}(\omega') d\omega d\omega' |\overline{+}\rangle_{\omega_s}|\overline{+}\rangle_{\omega_i}.\end{aligned} \tag{43}$$

After performing the integral over time variables, we obtain the wave function

$$\begin{aligned}&|\psi\rangle_2 \\ &= \iint d\omega_s d\omega_i G_{\Delta\omega_p}(\omega_+) G_{\Delta\omega_-}(\omega_-) G_{\delta\omega}(\omega_s) G_{\delta\omega}(\omega_i) |\omega_s, \omega_i\rangle,\end{aligned} \tag{44}$$

where we have defined $\omega_\pm = \frac{\omega_s \pm \omega_i}{2}$. The full calculation is detailed in Appendix A. The states described by Eq. (44) are noisy frequency-entangled states, displaying an elliptical joint spectral intensity in the (ω_+, ω_-) basis. The ellipticity R of the joint spectral intensity determines how entangled the state is.

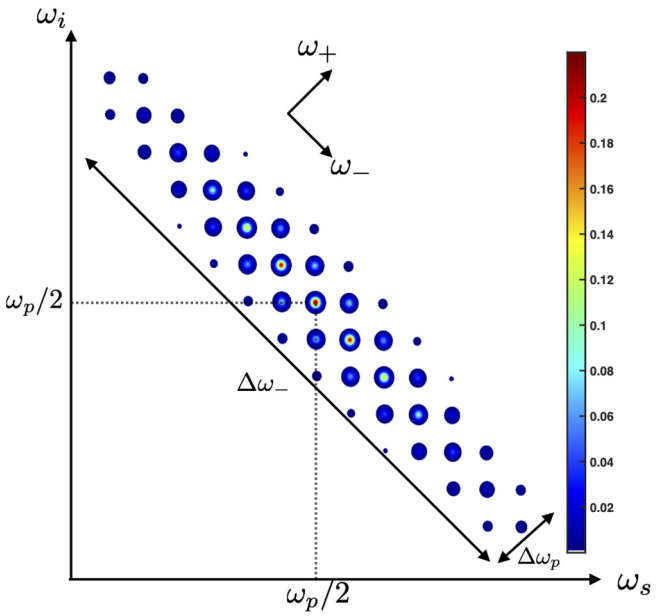

FIG. 2. Numerical simulation of the joint spectral intensity for a two-photon source in an optical cavity using arbitrary units. The size of the ellipse is delimited by the energy conservation (with a frequency width $1/\Delta\omega_p$) and the phase-matching condition (with a frequency width of $1/\Delta\omega_-$). The center of the ellipse corresponds to frequency degeneracy. Here the state is said to be anticorrelated since $\Delta\omega_- > \Delta\omega_p$.

It is defined as $R = \frac{1/\Delta\omega_-^2 - 1/\Delta\omega_p^2}{1/\Delta\omega_-^2 + 1/\Delta\omega_p^2}$, and the time noise in axis ω_- and ω_+ plays a role in the correlation-anticorrelation of the photons. A state with an arbitrary positive ellipticity is represented in the numerical simulation Fig. 2. Note that such biphoton state can be produced with an integrated chip in a transverse pump configuration [40,41]. In Fig. 3, we recap in a quantum circuit representation all the time-frequency gates which act on the initial ideal time-frequency GKP state.

IV. PRODUCTION AND MANIPULATION OF TIME-FREQUENCY GRID STATE

We are now ready to apply the previous definitions to describe the spectrum of a photon pair generated by spontaneous parametric down conversion (SPDC) in a nonlinear optical cavity. We will focus on a specific platform in order to perform both a detailed numerical study and the experimental illustration of our results, and also to study its application to measurement-based error correction.

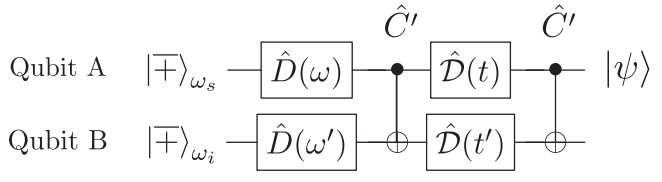

FIG. 3. Quantum circuit representing the generation of entangled 2D time-frequency GKP state.

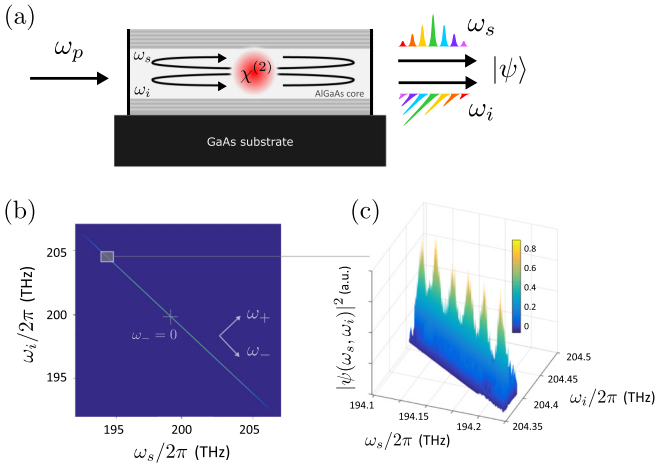

FIG. 4. (a) A pump beam illuminates an AlGaAs waveguide where photon pairs are generated by SPDC. The refractive index contrast between AlGaAs and air creates a cavity around the nonlinear medium, as the waveguide's facets play the role of mirrors. (b) Simulated joint spectral intensity of the state emitted by the nonlinear cavity, using the nominal structure of the device. (c) Experimental joint spectral intensity (detail).

A. Presentation of the integrated device for the generation of time-frequency GKP state

The device we consider here consists of an AlGaAs Bragg reflector waveguide emitting pairs of orthogonally polarized photons in the telecom band by type II SPDC. The working principle of the device is sketched in Fig. 4(a) [42]. The device is pumped with a continuous wave laser at $\lambda_p = 764$ nm having a linewidth $\Delta\omega_p = 2\pi \times 100$ kHz, much smaller than the phase-matching bandwidth and the free spectral range. This leads to the generation of strongly anticorrelated photon pairs over a spectral band of $2\pi \times 10.9$ THz centered around the frequency degeneracy as shown in the numerical simulations reported in Fig. 4(b). Moreover, the refractive index contrast between the semiconductor nonlinear medium and the air induces a Fabry-Perot effect, resulting in a built-in cavity. The free spectral range of the cavity is $\overline{\omega} = 2\pi \times 19.2$ GHz, yielding a comblike spectrum with approximatively 570 peaks. Figure 4(c) shows the measurement of a portion of the joint spectral intensity via stimulated emission tomography [40], evidencing a frequency comb structure.

The generated two-photon state can be written as

$$|\psi\rangle = \iint d\omega_s d\omega_i F(\omega_s, \omega_i)|\omega_s\rangle|\omega_i\rangle, \tag{45}$$

where the F is the product of four terms:

$$F(\omega_s, \omega_i) = f_+(\omega_+) f_-(\omega_-) f_{\text{cav}}(\omega_s) f_{\text{cav}}(\omega_i). \tag{46}$$

The function f_+ is related to the conservation of the energy, while f_- is related to the phase-matching condition. Both functions can be modeled as Gaussian functions. The effect of the cavity on each mode (signal and idler) is taken into account by the cavity functions $f_{\text{cav}}(\omega_{s(i)})$ that act as an imperfect frequency filter. We will assume that the cavity function is a sum of Gaussians, which is a good approximation

in the limit of a high-finesse cavity:

$$f_{\mathrm{cav}}(\omega) = \sum_{n\in\mathbb{Z}} T_n(\omega), \tag{47}$$

where again $T_n(\omega) = \exp(-(\omega - n\overline{\omega})^2/(2\delta\omega^2))$. The frequency width $\delta\omega$ depends on the finesse of the cavity. For a high-finesse cavity, we have $\overline{\omega} \gg \delta\omega$, and the two-photon state can be written as

$$|\psi\rangle = \sum_{n,m} \iint d\omega_s d\omega_i f_+(\omega_+) f_-(\omega_-) T_n(\omega_s) T_m(\omega_i) |\omega_s\rangle |\omega_i\rangle. \tag{48}$$

The resulting state is analogous to a grid state because of the cavity functions. We point out that states described by Eqs. (48) and (44) are equal, justifying the interpretation in terms of GKP states as depicted in Fig. 2.

It is interesting to notice that in the case where $G_{\Delta\omega_p}(\omega_+) = \delta(\omega_+)$ and $\overline{\omega}/\delta\omega \ll 1$, we can approximate $|\psi\rangle = \widetilde{|\bar{+}\rangle|\bar{+}\rangle} \simeq \hat{C}'|\tilde{+}\rangle|\tilde{+}\rangle$, where we used Eqs. (40) and (41). In this case, $|\psi\rangle$ is anticorrelated, and $\Delta\omega_p \ll \Delta\omega_-$. The joint spectral intensity is shown in Fig. 4(b) and it is close to a line along the ω_- direction. We thus have that $F(\omega_s, \omega_i) \simeq \delta(\omega_+ - \omega_p) f_-(\omega_-) f_{\mathrm{cav}}(\omega_s) f_{\mathrm{cav}}(\omega_i)$ and integration over ω_+ in Eq. (48) leads to

$$|\psi\rangle = \int d\omega_- f_-(\omega_-) f_{\mathrm{cav}}\left(\frac{\omega_p + \omega_-}{2}\right) f_{\mathrm{cav}}\left(\frac{\omega_p - \omega_-}{2}\right) \times \left|\frac{\omega_p + \omega_-}{2}, \frac{\omega_p - \omega_-}{2}\right\rangle. \tag{49}$$

This state is the one produced experimentally whose joint spectral intensity is represented on Fig. 4.

To summarize, the generation of 2D time-frequency GKP state can be apprehended in two ways. The first and usual one (described in Ref. [43], for instance) is to consider a pump beam which crosses a nonlinear crystal and generates by SPDC two photons, called signal and idler. The ellipticity of the joint spectral intensity quantifies the level of frequency entanglement and the optical cavity resonances determines the frequencies of both photons. The second interpretation provided in this paper is to consider the generation of the 2D physical time-frequency GKP state from fictitious 2D ideal time-frequency GKP state entangled by the time-frequency noise model described by Eq. (43).

B. Applications on time-frequency quantum error correction

The previously described 2D entangled time-frequency GKP state can be used to implement a measurement-based error-correction protocol, which was previously defined for quadrature position-momentum continuous variables [13,44].

In this scenario, the result of a measurement performed on one qubit (say, B, encoded in the idler photon, also called the ancilla) is used to correct the error on the other qubit A, encoded in the signal photon, also called the data qubit).

We will consider the effect of a time measurement on the ancilla qubit of state Eq. (48). Since both qubits are entangled, measuring the ancilla qubit (B) has an effect on the data qubit (A), as shown in Fig. 5 [4]. The operation realized in qubit B is teleported to qubit A, up to a known displacement on qubit A, which is given by the result of the measurement performed in qubit B. In the spirit of QEC, the interest of this approach is that, if noise corresponds to displacements in conjugate variables, as it is the case in the GKP code, one can show that, if qubit B is measured in one variable (time or frequency), its error in the measured variable is teleported to qubit A's error in the same variable. Thus, if qubit B's error is smaller than A's, this scheme can be used to decrease the noise in physical GKP states of A [44].

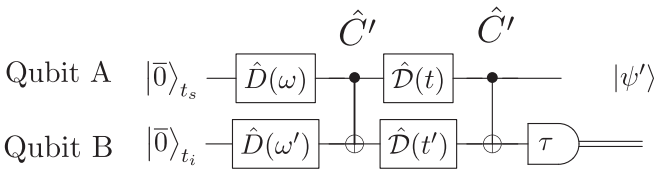

FIG. 5. The data qubit (signal) in arm A and the ancilla one (idler) in arm B are prepared in state $|\bar{+}\rangle_{\omega_s}|\bar{+}\rangle_{\omega_i} = |\bar{0}\rangle_{t_s}|\bar{0}\rangle_{t_i}$. After displacements and the $\hat{C}'$ gate, we perform a time measurement on the ancilla.

While the described protocol is very general, the QEC of GKP states requires a specific ordering of optical elements. This protocol allows for the correction of small displacements in phase space, for which the GKP is designed to be robust due to its comb structure. For the time-frequency GKP states that we consider in this paper, the small displacement shifts are due to temporal broadening in a dispersive medium and can cause an overlap between the $|\tilde{0}\rangle_t$ and $|\tilde{1}\rangle_t$ peaks of the logical qubit state. The correctability (the "small" displacement which occurs) of the GKP states is quantified thanks to a figure of merit developed in Refs. [38,45].

An interesting aspect of using measurement-based techniques is that they provide an alternative to a deterministic two-qubit gate in single-photon-based devices. As a matter of fact, implementing deterministic gates is a challenge in such setups, and starting from useful entangled resources can help achieving determinacy in different protocols. Possible ways to scale up the generation of time-frequency GKP states would be using on-demand production of pure single-photon states, reviewed in Ref. [46], for instance. Such ideas can be combined to implement efficient frequency gates, which are currently realized with electro-optic modulators and pulse shapers [28,47].

We expect that the fast technological evolution of the integrated circuits physics will enable effective photon-photon interaction with higher probability in the near future.

C. Experimental manipulation of time-frequency grid state and state detection

In this section, we study the implementation of a single qubit gate $\hat{\mathbf{Z}}_{t_s}$ on the state described by Eq. (49).

A possibility to manipulate frequency states is using electro-optical modulation (EOM) [28] for frequency-bin encoded qubits. Such techniques can also be used in the present context, with the difference that while in Ref. [28] each frequency is manipulated independently, in the present encoding redundancy is a key aspect, and qubit manipulation

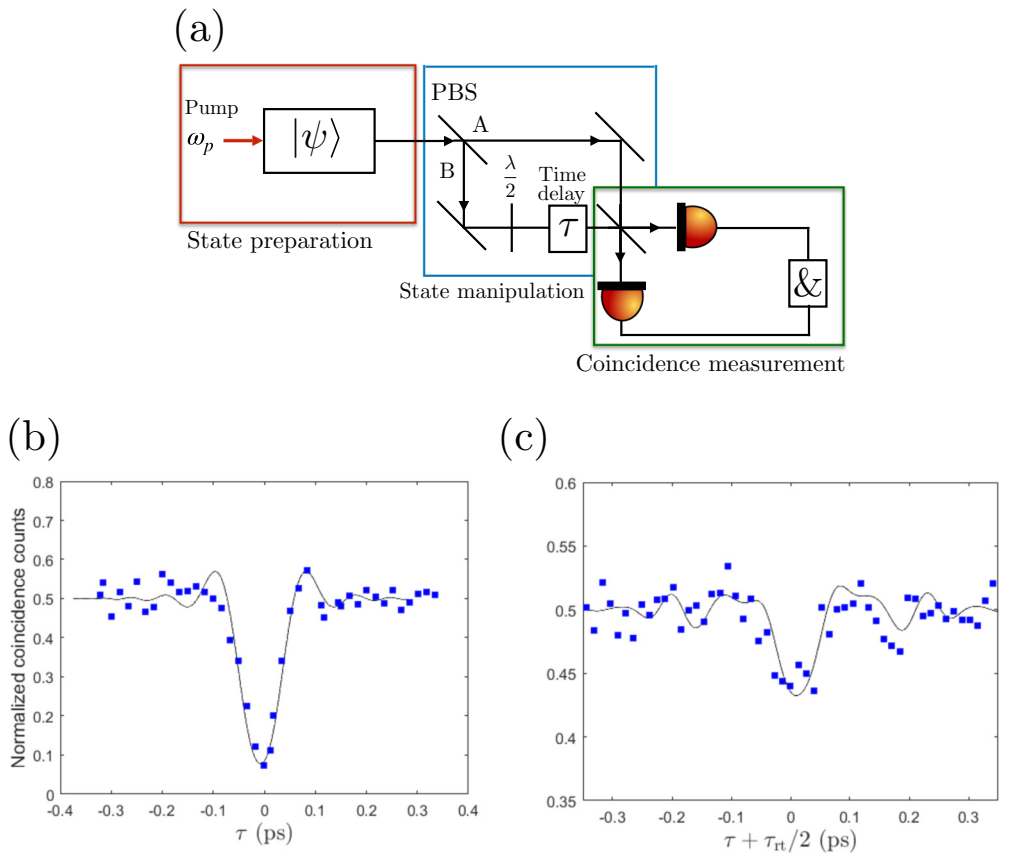

FIG. 6. (a) Hong-Ou-Mandel experiment enabling state manipulation and measurement. After being generated, signal and idler photons are separated with a polarizing beam splitter (PBS) and sent into two different arms of a HOM interferometer. In order to have the same polarization for the photons, a half-wave plate is added. Time delay (τ) in one arm performs a $\hat{\mathbf{Z}}_{t_s}$ gate for $\tau = -\tau_{rt}/2$. State measurement can be done by recombining both photons in a second beam splitter and performing coincidence measurements for different values of τ. (b) Experimental coincidence measurements corresponding to the state $|\bar{+}\rangle|\bar{+}\rangle$. (c) Experimental coincidence measurements corresponding to the state $|\bar{-}\rangle|\bar{+}\rangle$. The continuous lines are the result of numerical calculations taking into account the effects of birefringence, reflectivity, and chromatic dispersion in the AlGaAs chip.

requires acting on the whole frequency comb. It must then be manipulated as a whole, a situation that does not add any experimental complexity to the techniques considered in Ref. [28].

Interestingly, using EOM is not strictly necessary to manipulate time-frequency GKP states. We demonstrate here an experimentally simpler way to implement a quantum gate $\hat{\mathbf{Z}}_{t_s}$ for time-frequency GKP states and obtain a signature of the manipulation using a Hong-Ou-Mandel (HOM) interferometer [29,48] that can be used for state measurement, as detailed in the following. The HOM setup is sketched in Fig. 6(a): Signal and idler photons are sent to different arms of an interferometer, A and B. We consider them to be in the limit $\Delta\omega_p \ll \Delta\omega_-$ for simplicity. When we introduce a time delay τ between the two arms, the two photons acquire a phase difference such that the biphoton state arriving in the recombining beam splitter is given by

$$|\psi(\tau)\rangle = \int d\omega_- e^{-i(\omega_- + \omega_p)\tau/2} f_-(\omega_-) f_{\rm cav}\left(\frac{\omega_p+\omega_-}{2}\right) \times f_{\rm cav}\left(\frac{\omega_p-\omega_-}{2}\right) \left|\frac{\omega_p+\omega_-}{2}, \frac{\omega_p-\omega_-}{2}\right\rangle. \quad (50)$$

Without loss of generality for the present purposes, we consider $g(\omega_-) = f_-(\omega_-) f_{\rm cav}(\frac{\omega_p+\omega_-}{2}) f_{\rm cav}(\frac{\omega_p-\omega_-}{2})$ to be real. This function is also symmetric with respect to $\omega_- = 0$. The phase $e^{-i\omega_-\tau}$ corresponds to a displacement of τ in time, the conjugate variable to ω_-, as shown in Sec. III. It corresponds to the application of the $\hat{\mathcal{D}}_s(\tau)$ operator to the signal photon *before* the entangling operation.

By choosing $\tau = -\tau_{rt}/2$, the nth peaks of $g(\omega_-)$ with n even, remain unchanged, while for n odd, they gain a π phase and change signs, implementing the gate $\hat{\mathbf{Z}}_{t_s}|\bar{+}\rangle_{\omega_s} = |\bar{-}\rangle_{\omega_s}$ with a simple interferometric configuration and coincidence detection. Consequently, before its arrival on the HOM recombining beam splitter, the two-photon state can be written as $|\psi'\rangle = \widetilde{|\bar{-}\rangle|\bar{+}\rangle}$.

The signature of time displacement operator and the orthogonality of the two states can be detected by measuring temporal correlations with a HOM interferometer. As shown in Refs. [49,50], the HOM experiment is a direct measurement of the chronocyclic Wigner distribution of the phase-matching part of the joint spectral amplitude. The first experimental demonstration of these ideas can be found in Ref. [51]. In the experimental

context discussed here, it gives access to a cut in the time-frequency phase space of the Wigner function associated to the global variable ω_-, $W(\mu,\tau)$, where μ is the amplitude of displacement of ω_- and τ is the amplitude of displacement in time. The HOM experiment corresponds thus to a cut along the $\mu = 0$ line, where τ is varied. The partial information obtained is enough to distinguish between the two orthogonal states.

We have implemented the setup sketched in Fig. 6(a) on the state produced by our AlGaAs device presented in Sec. IV A. The two output ports of the beam splitter are connected to single-photon detectors (idQuantique ID230), which are free-running InGaAs/InP avalanche photodiodes whose efficiency is set to 25% and have a dead time of 25 μs. A time-to-digital converter (QuTau QuTools) measures the time differences between the detection events of each detector in a start-stop configuration with a temporal bin size of 81 ps. For $\tau = 0$, we expect a coincidence dip with a visibility fixed by the degree of indistinguishability between the signal and idler photons: This corresponds to the state $\hat{C}'|\tilde{+}\rangle_{\omega_s}|\tilde{+}\rangle_{\omega_i}$. For $\tau = -\tau_{\rm rt}/2$, we expect to observe a replica of the previous dip whose visibility is related to a combination of facets reflectivity, birefringence, and chromatic dispersion: This corresponds to the state $\hat{C}'\hat{\mathbf{Z}}_{t_s}|\tilde{+}\rangle_{\omega_s}|\tilde{+}\rangle_{\omega_i}$. The results of the corresponding measurements are shown respectively in Figs. 6(b) and 6(c). In the first [Fig. 6(b), in the vicinity $\tau = 0$] the visibility is 86%, while in the second case [Fig. 6(c), around $\tau = -\tau_{\rm rt}/2$], we obtain a visibility of 12%, making these two states well distinguishable.

We show in Appendix B numerical simulations of the visibility of the second dip of the HOM experiment as a function of the cavity reflectivity and for different bandwidths of the filters placed before the beam splitter. A visibility higher than 80% for the adjacent dips from the central dip can be obtained by improving the reflectivity of the facets and filtering the produced spectrum, which would decrease the number of exploitable peaks and reduce the detection rate but would still keep them of the order of a hundred.

Further possible manipulation of the time-frequency grid state has been proposed in Ref. [42], where tuning the pump frequency allows to engineer the joint spectral amplitude symmetry. Compared to other schemes where each comb line is manipulated individually [47,52], this technique enables us to address the odd and the even peaks collectively with low optical losses. In the formalism developed in Sec. II, the pump tuning corresponds to a frequency displacement operation on the signal and idler photons (see Fig. 2 of Ref. [42]), namely to nonlinear operation without the need to introduce a nonlinear material or EOM after the generation of the two-photon state.

D. Experimental proposal for quantum error correction in time-frequency variable

We now discuss the experimental feasibility of the time quantum error correction. The joint temporal intensity of the state given by Eq. (48) is represented in Fig. 7. The state is periodic, with periodicity of $2\pi/\overline{\omega} = 50$ ps using the parameters of the above-described source, along the two orthogonal directions $t_\pm$. But since the inverse of the energy conservation width $1/\Delta\omega_+$ is much larger than the cavity round-trip time $\tau_{\rm rt}$, the periodicity along the t_+ is not visible. A time measurement of the idler photon leads to a random temporal distribution which corresponds to the different peaks along the t_- axis. A single-photon detector should have 50-ps temporal resolution to distinguish these peaks, which is possible with current technology. Once the state is measured, further time or frequency correction operators could be applied on the data [38].

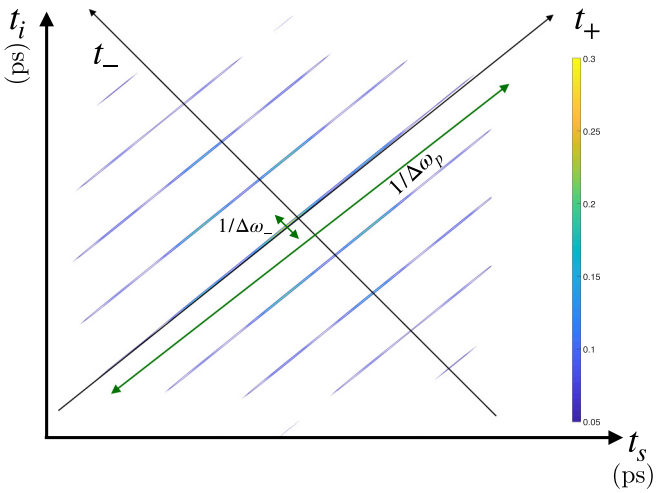

FIG. 7. Numerical simulation of the joint temporal intensity of the time-frequency GKP states in the case $\Delta\omega_- \gg \Delta\omega_p$ with a 50-ps periodicity. It corresponds to the Fourier transform of the state shown in Fig. 4(b). The state is periodic in both directions, but since the $1/\Delta\omega_p \gg 2\pi/\overline{\omega}$, we cannot see the periodicity in the t_+ direction since the data qubit is very noisy.

Error correction is also possible in frequency degrees of freedom, and it requires measuring one of the photons in the $\omega_\pm$ variables. This operation could be performed with nonlinear devices implementing a controlled quantum gate in the frequency degrees of freedom.

V. CONCLUSION

We detailed a formalism establishing the analogy between continuous variables consisting of many modes of single photons and those associated to a single mode field's quadratures. We introduced a rigorous construction and provided a physical and mathematical meaning to the chronocyclic Wigner distribution in a quantum optics experiment. Using the introduced formal analogies, we showed that experimental setups consisting of a SPDC source and a filtering cavity can be a natural source of time-frequency GKP states, which are time-frequency non-Gaussian states useful for fault-tolerant quantum protocols manipulating continuous variables. Qubits can be encoded in frequency and time degrees of freedom of photons and entangled GKP states can be generated and manipulated. We have experimentally illustrated these results in an integrated optical platform. Finally, we have shown that the produced state is a resource for measurement based quantum computing (MBQC) and error correction, and both can be implemented through time or frequency measurement of one photon of the pair. A natural perspective is to combine our results with already existing

technologies for quantum photonic circuits for further applications and scaling [53–56]. Using the measurement-based principle, other protocols involving quadrature position-momentum GKP states could be generalized to time-frequency variables such as the correction of Gaussian errors using GKP states as a non-Gaussian resource with the two-mode GKP repetition code [12,57].

ACKNOWLEDGMENTS

The authors gratefully acknowledge ANR (Agence Nationale de la Recherche) for the financial support of this work through Project SemiQuantRoom (Project No. ANR-14-CE26-0029) and through Labex SEAM (Science and Engineering for Advanced Materials and devices) Projects No. ANR-10-LABX-0096 and No. ANR-18-IDEX-0001. The French RENATECH network and Université Sorbonne Paris Cité for a doctoral fellowship to G.M. are also warmly acknowledged. A.K. acknowledges support by the Georg H. Endress Foundation.

APPENDIX A: CALCULATION OF THE WAVE FUNCTION OF 2D TIME-FREQUENCY ENTANGLED GKP STATES WITH THE TIME-FREQUENCY NOISE MODEL

In this section, we detail the calculation of the 2D entangled time-frequency GKP states from the time-frequency noise model described in Sec. III C 2.

We start by applying the unitary operator describing the uncorrelated frequency noise between the signal and the idler fictitious ideal time-frequency GKP states: $|\psi_1\rangle = \iint \hat{D}_s(\omega)\hat{D}_i(\omega')G_{\delta\omega}(\omega)G_{\delta\omega}(\omega')d\omega d\omega'|\overline{+}\rangle_{\omega_s}|\overline{+}\rangle_{\omega_i}$. After applying the frequency displacement operator, we obtain the wave function

$$|\psi_1\rangle = \left[\iint G_{\delta\omega}(\omega)G_{\delta\omega}(\omega')d\omega d\omega'\right] \times \sum_{n,m} |n\overline{\omega}+\omega\rangle|m\overline{\omega}+\omega'\rangle. \tag{A1}$$

The entangling gate described by Eq. (42), which equivalently corresponds to a correlated time noise, is then applied on the previous state:

$$|\psi_2\rangle = \left(\iint \hat{\mathcal{D}}_s\left(\frac{t+t'}{2}\right)\hat{\mathcal{D}}_i\left(\frac{t-t'}{2}\right)G_{1/\Delta\omega_p}(t) \times G_{1/\Delta\omega_-}(t')dtdt'\right)|\psi_1\rangle. \tag{A2}$$

The time displacement operators are then applied:

$$|\psi_2\rangle = \iint G_{1/\Delta\omega_p}(t)\times G_{1/\Delta\omega_-}(t')dtdt' \times \iint G_{\delta\omega}(\omega)G_{\delta\omega}(\omega')d\omega d\omega' \times \sum_{n,m} e^{i(n\overline{\omega}+\omega)(t+t')/2}e^{i(m\overline{\omega}+\omega)(t-t')/2}|n\overline{\omega}+\omega\rangle|m\overline{\omega}+\omega'\rangle. \tag{A3}$$

We then integrate over the time variables, using the Fourier transform of Gaussian function:

$$\int dt G_{1/\Delta\omega_p}(t)e^{i[(n+m)\overline{\omega}+\omega+\omega']t/2} = G_{\Delta\omega_p}\left[\frac{(n+m)\overline{\omega}+\omega+\omega'}{2}\right]. \tag{A4}$$

We thus obtain the following wave function:

$$|\psi_2\rangle = \iint \sum_{n,m} G_{\Delta\omega_p}\left(\frac{(n+m)\overline{\omega}+\omega+\omega'}{2}\right)G_{\delta\omega}(\omega)G_{\delta\omega}(\omega') \times G_{\Delta\omega_-}\left(\frac{(n-m)\overline{\omega}+\omega-\omega'}{2}\right)d\omega d\omega'|n\overline{\omega}+\omega\rangle|m\overline{\omega}+\omega'\rangle. \tag{A5}$$

A final frequency variables change gives

$$|\psi_2\rangle = \iint G_{\Delta\omega_p}(\omega_+)G_{\Delta\omega_-}(\omega_-)G_{\delta\omega}(\omega-n\overline{\omega}) \times G_{\delta\omega}(\omega'-m\overline{\omega})d\omega d\omega'|\omega\rangle|\omega'\rangle, \tag{A6}$$

which corresponds to Eq. (48) and the wave function of the state created by SPDC described by Eq. (44).

APPENDIX B: IMPLEMENTING GATES USING THE HONG-OU-MANDEL EXPERIMENT

1. Implementing the $\hat{\mathbf{Z}}$ for the time-frequency GKP states

In this section, we detail how to implement the single-qubit gate $\hat{\mathbf{Z}}$ for the time-frequency GKP states. The frequency ω_p is taken different from zero. For simplicity, we will describe the principle of the gate for an ideal GKP state. Starting from the Eq. (49) and supposing that each photon goes to one arm of a Hong-Ou-Mandel (HOM) interferometer where a linear medium was inserted in one of the arms (see Fig. 6), the wave function can be written, after the beam splitter, taking into account only the coincidence terms as

$$|\psi\rangle_\tau = \frac{1}{2}\int d\omega_- f_-(\omega_-)f_{\text{cav}}\left(\frac{\omega_p+\omega_-}{2}\right)f_{\text{cav}}\left(\frac{\omega_p-\omega_-}{2}\right) \times e^{-i\frac{(\omega_p+\omega_-)\tau}{2}}\left(\left|\frac{\omega_p+\omega_-}{2},\frac{\omega_p-\omega_-}{2}\right\rangle - \left|\frac{\omega_p-\omega_-}{2},\frac{\omega_p+\omega_-}{2}\right\rangle\right), \tag{B1}$$

where τ is the temporal delay introduced by the linear medium in the upper path. After performing a change of variable, we obtain

$$|\psi\rangle_\tau = \frac{1}{2}\int d\omega_-\left(f_-(\omega_-)e^{-i\frac{\omega_-\tau}{2}} - f_-(-\omega_-)e^{+i\frac{\omega_-\tau}{2}}\right) \times f_{\text{cav}}\left(\frac{\omega_p+\omega_-}{2}\right)f_{\text{cav}}\left(\frac{\omega_p-\omega_-}{2}\right) \times \left|\frac{\omega_p+\omega_-}{2},\frac{\omega_p-\omega_-}{2}\right\rangle. \tag{B2}$$

In the last equation, we discard an unimportant global phase. The coincidence probability $I(\tau) = \iint d\omega_s d\omega_i |\langle \omega_s, \omega_i | \psi \rangle_\tau|^2$ reads

$$I(\tau) = \frac{1}{2}\left\{1 - \frac{1}{N}\mathrm{Re}\left[\int \left| f_{\mathrm{cav}}\left(\frac{\omega_p + \omega_-}{2}\right) f_{\mathrm{cav}}\left(\frac{\omega_p - \omega_-}{2}\right)\right|^2 \right.\right.$$
$$\left.\left. \times\ f_-(\omega_-) f_-^*(-\omega_-) e^{-i\omega_-\tau/2} d\omega_- \right]\right\}, \qquad \text{(B3)}$$

where $N = \int |f_{\mathrm{cav}}(\frac{\omega_p+\omega_-}{2}) f_{\mathrm{cav}}(\frac{\omega_p-\omega_-}{2})|^2 f_-(\omega_-) f_-^*(-\omega_-) d\omega_-$. In Ref. [50], it was shown that the coincidence probability is proportional to a cut of the chronocyclic Wigner distribution at $\omega_- = 0$. We can then only partially characterize the state, but the information obtained is enough to analyze different time-frequency GKP states.

Experimentally, we realize the HOM experiment having as initial state (49), so that we can observe the effect of the gate $\hat{\mathbf{Z}}_{\mathbf{t_s}}$. For $\tau = -\tau_{\mathrm{rt}}/2$, the odd peaks of state (49) gain a negative amplitude, which means that a $\hat{\mathbf{Z}}_{\mathbf{t_s}}$ gate was implemented. This corresponds to the transformation $\hat{\mathbf{Z}}_{t_s}|\mp\rangle_{\omega_s}$ applied to the ideal GKP state, which means that the physical state is transformed according to $|\widetilde{\mp}\rangle|\widetilde{\mp}\rangle \rightarrow |\widetilde{-}\rangle|\widetilde{\mp}\rangle$.

Here, we perform the analytical calculation for the coincidence probability of the state, for a high reflectivity of the cavity and without taking into account the birefringence and the chromatic dispersion. Assuming that $\overline{\omega}/\delta\omega \gg 1$, we have

$$I(2\tau) = \frac{1}{2}\left[1 - e^{-\tau^2\delta\omega^2/2} \sum_{n=-d}^{d} \alpha_n \cos(n\overline{\omega}\tau)\right], \qquad \text{(B4)}$$

where d is the number of peaks, $\frac{1}{N} = \frac{1}{\sum_{n=-d}^{d}\alpha_n}$, and $\alpha_n = e^{-(\frac{\omega_p}{2} - n\overline{\omega})^2/\delta\omega^2}$. In Figs. 8(a) and 8(b), we show the plot of the coincidence probability with arbitrary units for a cavity with a reflectivity of $r = 0.9$. The HOM interference exhibits a replica [48], and depending on the time displacement we perform, we obtain for the signal photon the state $|\widetilde{\mp}\rangle_{\omega_s}$ or $|\widetilde{-}\rangle_{\omega_s}$. The visibility of the central dip and the nearest replica are too close to distinguish the two states, contrary to the experimentally studied case where low reflectivity and chromatic dispersion increase the coincidence probability of the state $|\widetilde{-}\rangle_{\omega_s}$. For a high reflectivity of the cavity, to distinguish the two orthogonal states, we then have to choose two replicas away from the central dip.

2. Numerical simulations of the visibility of the second dip of the HOM experiment

We now present the visibility of the secondary dip from the central one with respect to the reflectivity of the facets in our specific AlGaAs device. The intersection of the dashed lines indicates the conditions in which the experiment has been performed: a modal reflectivity of the facets of 0.3 without frequency filters, which leads to a theoretical prediction of 15% of visibility, which is in good agreement with the experimentally observed result of 12%; see Fig. 6(c). Such visibility is enough to distinguish both possible GKP states. Note that the visibility of the second dip can be increased by depositing a reflective coating on the facets, but this solution would equally enhance the detrimental effect of the cavity birefringence by making peaks corresponding to different polarizations more distinguishable. In addition to coating, a potential strategy to improve the visibility is to add frequency filters in order to select the central part of the spectrum and reduce the effect of birefringence and chromatic dispersion. For instance, the total frequency bandwidth for about 500 peaks is 70 nm as shown in Fig. 9. For each curve in Fig. 9, we note that the visibility reaches a maximum and then decreases when increasing the reflectivity, well illustrating our discussion on the antagonist roles of the reflectivity and the birefringence. It shows that a visibility of the order of 80% is well on reach.

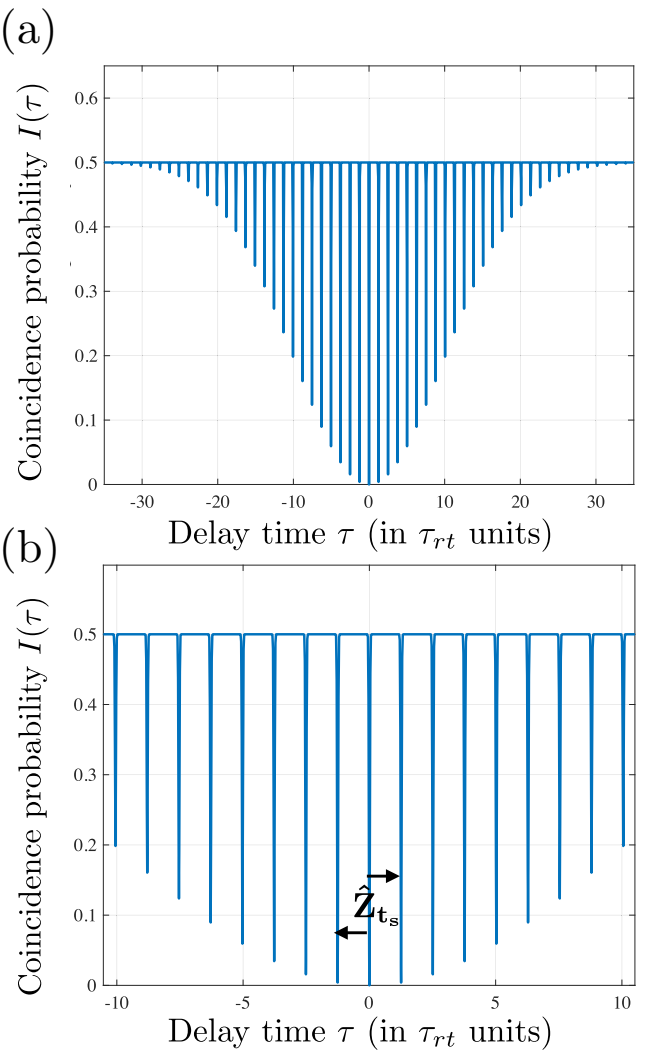

FIG. 8. (a) Numerical simulation of the HOM experiment for the two-photon state for a highly reflective cavity without taking into account the birefringence and the chromatic dispersion. Coincidence probability as a function of the delay in units of τ_{rt}. Selecting $\tau = \pm\tau_{\mathrm{rt}}/2$ performs a $\hat{\mathbf{Z}}_{\mathbf{t_s}}$ gate. (b) Detail of panel (a).

APPENDIX C: QUANTUM ERROR CORRECTION

We now consider the situation where the widths of the phase matching and energy conservation conditions are finite and the state obtained corresponds to an ellipse in the

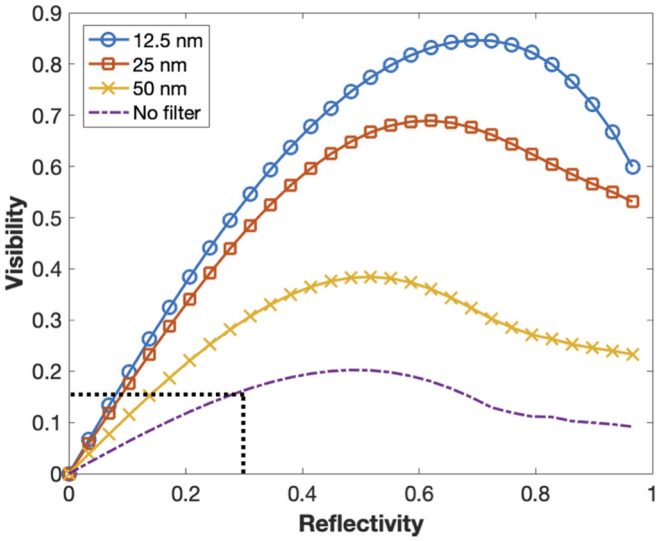

FIG. 9. Numerical simulation of the visibility of the secondary peaks, nearest to the central dip, as a function of the reflectivity of the facets for different bandwidth of the frequency filters placed before the beam splitter. The birefringence and the chromatic dispersion are here taken into account. The intersection of the two dashed lines indicates the conditions of the realized experiment whose coincidence measurement is presented in Fig. 6(c).

joint spectral intensity plane, as discussed in Sec. IV. As mentioned, in this situation we have an entangled GKP state in time. We can consider that one of the photons, say, the idler, plays the role of the ancilla while the signal one is the data qubit in a measurement-based circuit as in Fig. 5. We will thus perform a measurement in the ancilla (frequency or time measurement) and use the measurement result to correct the data qubit, as in Refs. [4].

1. Correction against temporal shift (MBQC)

The principle of the MBQC is the following: We prepare an entangled GKP state, noisy in time and frequency [Eq. (48)], which can be prepared with a SPDC source in an optical cavity as shown in the main text. Then we perform a time or frequency measurement on the qubit ancilla in a particular basis. Since only the time noise is entangled [see Eq. (42)], the time measurement provides the information about this displacement (see Fig. 5).

We then report the same procedures as in Ref. [4], assuming a Dirac distribution for the time and frequency noise, and investigate the influence of the time measurement of the ancilla on the time noise of the signal.

We start from a separable state, where the data (signal) and the ancilla (idler) are initialized in the frequency $|\overline{+}\rangle_{\omega_s}|\overline{+}\rangle_{\omega_i}$:

$$|\psi\rangle = |\overline{+}\rangle_{\omega_s}|\overline{+}\rangle_{\omega_i} = |\overline{0}\rangle_{t_s}|\overline{0}\rangle_{t_i} = \sum_{n,m\in\mathbb{Z}} |nT\rangle|mT\rangle, \tag{C1}$$

with $T = 2\pi\tau_{\rm rt}$. Frequency and time Dirac distribution noises are assumed for both qubits:

$$|\overline{0}\rangle_{t_s}|\overline{0}\rangle_{t_i} \to \hat{\mathcal{D}}_s(t)\hat{\mathcal{D}}_i(t')\hat{D}_s(\omega)\hat{D}_i(\omega')|\overline{0}\rangle_{t_s}|\overline{0}\rangle_{t_i}, \tag{C2}$$

and then time noises are entangled with the $\hat{C}'$ operation:

$$\begin{aligned}
&\hat{C}'\hat{\mathcal{D}}_s(t)\hat{\mathcal{D}}_i(t')\hat{C}'^{-1}\hat{D}_s(\omega)\hat{D}_i(\omega')|\overline{0}\rangle_{t_s}|\overline{0}\rangle_{t_i} \\
&= \hat{\mathcal{D}}_s\left(\frac{t+t'}{2}\right)\hat{\mathcal{D}}_i\left(\frac{t-t'}{2}\right)\hat{D}_s(\omega)\hat{D}_i(\omega')|\overline{0}\rangle_{t_s}|\overline{0}\rangle_{t_i} \\
&= \sum_{n,m} e^{in\omega T}e^{im\omega' T}\left|nT+\frac{t+t'}{2}\right\rangle\left|mT+\frac{t-t'}{2}\right\rangle.
\end{aligned} \tag{C3}$$

We realize a time measurement on the ancilla (the idler), so let us consider that the detector clicks at time τ, which can take only the values $\tau = \frac{t-t'}{2} + mT$. The initial state is projected into

$$|\overline{0}\rangle_{t_s} \to e^{i\omega'(\tau-\frac{t+t'}{2})}\hat{\mathcal{D}}_s\left(\frac{t+t'}{2}\right)\hat{D}_s(\omega)|\overline{0}\rangle_{t_s}. \tag{C4}$$

The temporal shift of the data qubit is entirely determined by the noise (shift) of the ancilla. The probability of success is given by $|t-t'| < \frac{\pi}{2\overline{\omega}}$, which means the probability to avoid a fall in another $\frac{\pi}{2\overline{\omega}}$ time window.

2. Gaussian distribution of the noise

Now we consider that the time and frequency noises obey a Gaussian distribution. We thus have the state, as written before Eq. (40),

$$|\psi\rangle = \left[\iint\iint G_{\delta\omega}(\omega)G_{\delta\omega}(\omega')G_{1/\Delta\omega_-}(t)G_{1/\Delta\omega_p}(t')\hat{\mathcal{D}}_s\left(\frac{t+t'}{2}\right)\hat{\mathcal{D}}_i\left(\frac{t-t'}{2}\right)\hat{D}_s(\omega)\hat{D}_i(\omega')dtdt'd\omega d\omega'\right]|\overline{0}\rangle_{t_s}|\overline{0}\rangle_{t_i}. \tag{C5}$$

We then apply the time and frequency displacement operators on the GKP state:

$$|\psi\rangle = \iint\iint G_{\delta\omega}(\omega)G_{\delta\omega}(\omega')G_{1/\Delta\omega_-}(t)G_{1/\Delta\omega_p}(t')\sum_{n,m\in\mathbb{Z}} e^{in\omega T}e^{im\omega T}\left|nT+\frac{t+t'}{2}\right\rangle\left|mT+\frac{t-t'}{2}\right\rangle dtdt'd\omega d\omega'. \tag{C6}$$

The joint temporal amplitude of the state $\langle t_s, t_i||\psi\rangle = H(t_s, t_i)$ is a circle whose radius is the frequency width $\overline{\omega}$, with elliptical peaks whose half axis are equal to $\Delta\omega_-$ and $\Delta\omega_p$; see Fig. 7. In the case where $\Delta\omega_- \gg \Delta\omega_p$, the joint temporal amplitude associated is a periodic (along t_-) set of lines along t_+.

We then perform a time measurement on the ancilla, a click is detected at time τ that can take the value $\tau = mT + \frac{t-t'}{2}$. The new wave function $|\psi'\rangle_\tau = \langle\tau||\psi\rangle$ is, after performing an integration over t and after normalization,

$$|\psi'\rangle_\tau = \int \left(\iint \sum_{n,m\in\mathbb{Z}} e^{i\omega nT} \frac{G_{\Delta\omega_-}(t' + 2(\tau - mT))G_{\Delta\omega_p}(t')}{G_{\sqrt{\Delta\omega_-^2+\Delta\omega_p^2}}(2(\tau - mT))} G_{\delta\omega}(\omega')G_{\delta\omega}(\omega)e^{i\omega' mT}|(n-m)T + \tau + t')\rangle d\omega dt' \right) d\omega'. \quad \text{(C7)}$$

After the time measurement of the ancilla (idler), the state is projected into a one-dimensional GKP state. The time noise distribution of the signal is updated,

$$\frac{G_{\Delta\omega_-}(t' + 2(\tau - mT))G_{\Delta\omega_p}(t')}{G_{\sqrt{\Delta\omega_-^2+\Delta\omega_p^2}}(2(\tau - mT))} = G_\delta(t' - t_m). \quad \text{(C8)}$$

It is a normal distribution with variance $\delta^2 = \frac{\Delta\omega_-^2\,\Delta\omega_p^2}{\Delta\omega_-^2+\Delta\omega_p^2}$ and mean value $t_m = \frac{\Delta\omega_-^2}{\Delta\omega_-^2+\Delta\omega_p^2}(\tau + mT)$. The time noise of the data depends on both the noises of the ancilla and the data.

Hence, the state can be written as

$$|\psi'\rangle_\tau = \sum_{m\in\mathbb{Z}} \int \iint d\omega dt' d\omega' G_{\delta\omega}(\omega)G_\delta(t' - t_m)G_{\delta\omega}(\omega')e^{i\omega' mT}\hat{D}_s(-mT + \tau + t')\hat{D}_s(\omega)|\overline{+}\rangle_{t_s}. \quad \text{(C9)}$$

We point out that for time-correlated photons with high noise in time variables $\Delta\omega_- \gg \Delta\omega_p$, the time distribution of the signal only depends on the noise of the idler, since $\delta \sim \Delta\omega_-$ and $t_m = \tau + mT$. Therefore, the analysis is the same than the previous section. We can understand this noise reduction on Fig. 7 as follows: When we perform a measurement on the t_- axis, the signal is projected into a less noisy state since the updated time distribution of the signal depends on the time distribution of the idler. As a consequence, according to (C8), the state becomes periodic along the t_+ direction, since the time width of each peak becomes $\Delta\omega_p$ (instead of $\Delta\omega_-$) which is smaller than $2\pi/\overline{\omega}$.

Note that if we had considered an anticorrelated initial state, error correction would be effective if the signal photon were detected, instead of the idler one.

[1] S. L. Braunstein and P. van Loock, Rev. Mod. Phys. **77**, 513 (2005).

[2] M. A. Nielsen and I. L. Chuang, *Quantum Computation and Quantum Information: 10th Anniversary Edition* (Cambridge University Press, Cambridge, UK, 2010).

[3] D. Gottesman, Phys. Rev. A **57**, 127 (1998).

[4] A. M. Steane, Phys. Rev. Lett. **77**, 793 (1996).

[5] D. Gottesman, Ph.D. thesis, Caltech, 1997, arXiv:quant-ph/9705052.

[6] C. Weedbrook, S. Pirandola, R. García-Patrón, N. J. Cerf, T. C. Ralph, J. H. Shapiro, and S. Lloyd, Rev. Mod. Phys. **84**, 621 (2012).

[7] D. F. Walls, Nature (London) **306**, 141 (1983).

[8] B. Chalopin, F. Scazza, C. Fabre, and N. Treps, Phys. Rev. A **81**, 061804(R) (2010).

[9] N. C. Menicucci, S. T. Flammia, and O. Pfister, Phys. Rev. Lett. **101**, 130501 (2008).

[10] H. Yonezawa, K. Nagashima, and A. Furusawa, Opt. Express **18**, 20143 (2010).

[11] D. Gottesman, A. Kitaev, and J. Preskill, Phys. Rev. A **64**, 012310 (2001).

[12] K. Noh, S. M. Girvin, and L. Jiang, arXiv:1903.12615 [quant-ph] (2019).

[13] B. Q. Baragiola, G. Pantaleoni, R. N. Alexander, A. Karanjai, and N. C. Menicucci, Phys. Rev. Lett. **123**, 200502 (2019).

[14] C. Vuillot, H. Asasi, Y. Wang, L. P. Pryadko, and B. M. Terhal, Phys. Rev. A **99**, 032344 (2019).

[15] H. M. Vasconcelos, L. Sanz, and S. Glancy, Opt. Lett. **35**, 3261 (2010).

[16] B. C. Travaglione and G. J. Milburn, Phys. Rev. A **66**, 052322 (2002).

[17] S. Pirandola, S. Mancini, D. Vitali, and P. Tombesi, EPL **68**, 323 (2004).

[18] A. Ourjoumtsev, A. Dantan, R. Tualle-Brouri, and P. Grangier, Phys. Rev. Lett. **98**, 030502 (2007).

[19] V. Averchenko, C. Jacquard, V. Thiel, C. Fabre, and N. Treps, New J. Phys. **18**, 083042 (2016).

[20] O. Morin, J. Liu, K. Huang, F. Barbosa, C. Fabre, and J. Laurat, J.Vis. Exp. **87**, 51224 (2014).

[21] C. Flühmann, T. L. Nguyen, M. Marinelli, V. Negnevitsky, K. Mehta, and J. P. Home, Nature (London) **566**, 513 (2019).

[22] P. Campagne-Ibarcq, A. Eickbusch, S. Touzard, E. Zalys-Geller, N. E. Frattini, V. V. Sivak, P. Reinhold, S. Puri, S. Shankar, R. J. Schoelkopf *et al.*, arXiv:1907.12487 [quant-ph] (2019).

[23] D. J. Weigand and B. M. Terhal, Phys. Rev. A **97**, 022341 (2018).

[24] K. R. Motes, B. Q. Baragiola, A. Gilchrist, and N. C. Menicucci, Phys. Rev. A **95**, 053819 (2017).

[25] M. Eaton, R. Nehra, and O. Pfister, arXiv:1903.01925 [quant-ph] (2019).

[26] F. Boitier, A. Orieux, C. Autebert, A. Lemaître, E. Galopin, C. Manquest, C. Sirtori, I. Favero, G. Leo, and S. Ducci, Phys. Rev. Lett. **112**, 183901 (2014).

[27] P. Wang, M. Chen, N. C. Menicucci, and O. Pfister, Phys. Rev. A **90**, 032325 (2014).

[28] J. M. Lukens and P. Lougovski, Optica **4**, 8 (2017).

[29] C. K. Hong, Z. Y. Ou, and L. Mandel, Phys. Rev. Lett. **59**, 2044 (1987).
[30] A. Royer, Phys. Rev. A **15**, 449 (1977).
[31] L. Maccone and K. Sacha, Phys. Rev. Lett. **124**, 110402 (2020).
[32] C. Brif and A. Mann, Phys. Rev. A **59**, 971 (1999).
[33] T. Tilma, M. J. Everitt, J. H. Samson, W. J. Munro, and K. Nemoto, Phys. Rev. Lett. **117**, 180401 (2016).
[34] J.-P. W. MacLean, S. Schwarz, and K. J. Resch, Phys. Rev. A **100**, 033834 (2019).
[35] K. B. Moller, T. G. Jorgensen, and G. Torres-Vega, J. Chem. Phys. **106**, 7228 (1997).
[36] K. Duivenvoorden, B. M. Terhal, and D. Weigand, Phys. Rev. A **95**, 012305 (2017).
[37] V. V. Albert, K. Noh, K. Duivenvoorden, D. J. Young, R. T. Brierley, P. Reinhold, C. Vuillot, L. Li, C. Shen, S. M. Girvin *et al.*, Phys. Rev. A **97**, 032346 (2018).
[38] S. Glancy and E. Knill, Phys. Rev. A **73**, 012325 (2006).
[39] S. Parker, S. Bose, and M. B. Plenio, Phys. Rev. A **61**, 032305 (2000).
[40] A. Eckstein, G. Boucher, A. Lemaitre, P. Filloux, I. Favero, G. Leo, J. E. Sipe, M. Liscidini, and S. Ducci, Laser Photon. Rev. **8**, L76 (2014).
[41] S. Francesconi, F. Baboux, A. Raymond, N. Fabre, G. Boucher, A. Lemaître, P. Milman, M. Amanti, and S. Ducci, Optica **7**, 316 (2020).
[42] G. Maltese, M. I. Amanti, F. Appas, G. Sinnl, A. Lemaître, P. Milman, F. Baboux, and S. Ducci, npj Quantum Inf. **6**, 13 (2020).
[43] M. Fiorentino, S. M. Spillane, R. G. Beausoleil, T. D. Roberts, P. Battle, and M. W. Munro, Opt. Express **15**, 7479 (2007).
[44] N. C. Menicucci, Phys. Rev. Lett. **112**, 120504 (2014).
[45] Y. Shi, C. Chamberland, and A. Cross, New J. Phys. **21**, 093007 (2019).
[46] P. Senellart, G. Solomon, and A. White, Nat. Nanotechnol. **12**, 1026 EP (2017).
[47] P. Imany, O. D. Odele, M. S. Alshaykh, H.-H. Lu, D. E. Leaird, and A. M. Weiner, Opt. Lett. **43**, 2760 (2018).
[48] Y. J. Lu, R. L. Campbell, and Z. Y. Ou, Phys. Rev. Lett. **91**, 163602 (2003).
[49] T. Douce, A. Eckstein, S. P. Walborn, A. Z. Khoury, S. Ducci, A. Keller, T. Coudreau, and P. Milman, Sci. Rep. **3**, 3530 (2013).
[50] G. Boucher, T. Douce, D. Bresteau, S. P. Walborn, A. Keller, T. Coudreau, S. Ducci, and P. Milman, Phys. Rev. A **92**, 023804 (2015).
[51] F. A. Beduini, J. A. Zielińska, V. G. Lucivero, Y. A. de Icaza Astiz, and M. W. Mitchell, Phys. Rev. Lett. **114**, 120402 (2014).
[52] H.-H. Lu, J. M. Lukens, B. P. Williams, P. Imany, N. A. Peters, A. M. Weiner, and P. Lougovski, npj Quantum Inf. **5**, 24 (2019).
[53] M. Stefszky, V. Ulvila, Z. Abdallah, C. Silberhorn, and M. Vainio, Phys. Rev. A **98**, 053850 (2018).
[54] M. Kues, C. Reimer, P. Roztocki, L. R. Cortés, S. Sciara, B. Wetzel, Y. Zhang, A. Cino, S. T. Chu, B. E. Little *et al.*, Nature (London) **546**, 622 (2017).
[55] J. Wang, S. Paesani, Y. Ding, R. Santagati, P. Skrzypczyk, A. Salavrakos, J. Tura, R. Augusiak, L. Mančinska, D. Bacco *et al.*, Science **360**, 285 (2018).
[56] C. P. Dietrich, A. Fiore, M. G. Thompson, M. Kamp, and S. Höfling, Laser Photon. Rev. **10**, 870 (2016).
[57] Q. Zhuang, J. Preskill, and L. Jiang, New J. Phys. **22**, 022001 (2020).